Global and Local Dynamics of High-Gamma Activity Underlying Error Processing in the Human Brain Revealed by Noninvasive and Intracranial EEG

Abbreviated title: High-Gamma Activity in Human Error Processing

Martin Völker[1,2,3,4], Lukas D.J. Fiederer[1,4,5,6*], Sofie Berberich[1,7*], Jiří Hammer[1,4,8*], Joos Behncke[1,3,4], Pavel Kršek[8], Martin Tomášek[8], Petr Marusič[8], Peter C. Reinacher[7,9], Volker A. Coenen[7,9], Andreas Schulze-Bonhage[4,7,10], Wolfram Burgard[3,4,11] and Tonio Ball[1,4,6,7]

1 - Translational Neurotechnology Lab, Medical Center – University of Freiburg, 79106 Freiburg, Germany
2 - Graduate School of Robotics, University of Freiburg, 79106 Freiburg, Germany
3 - Department of Computer Science, University of Freiburg, 79110 Freiburg, Germany
4 - BrainLinks-BrainTools, University of Freiburg, 79110 Freiburg, Germany
5 - Faculty of Biology, University of Freiburg, 79104 Freiburg, Germany
6 - Bernstein Center, University of Freiburg, 79104 Freiburg, Germany
7 - Faculty of Medicine, University of Freiburg, 79106 Freiburg, Germany
8 - Charles University, Second Faculty of Medicine, Motol University Hospital, 15006 Prague, Czech Republic
9- Stereotactic and Functional Neurosurgery, Medical Center – University of Freiburg, 79106 Freiburg, Germany
10 - Epilepsy Center, Medical Center – University of Freiburg, 79106 Freiburg, Germany
11 - Autonomous Intelligent Systems, University of Freiburg, 79110 Freiburg, Germany
* These authors contributed equally to this work.

Corresponding author: Martin Völker, Translational Neurotechnology Lab, Engelbergerstr. 21, 79106 Freiburg, Germany, email martin.voelker@uniklinik-freiburg.de

Number of pages: 39

Number of figures: 9

Number of tables: 1

Number of words in Abstract: 250

Number of words in Introduction: 647

Number of words in Discussion: 1441

Conflict of Interest: The authors declare no competing financial interests.

Acknowledgements: This work was supported by DFG grant EXC1086 BrainLinks-BrainTools, Baden-Württemberg Stiftung grant BMI-Bot, Graduate School of Robotics in Freiburg, Germany and the State Graduate Funding Program of Baden-Württemberg, Germany.

Abstract

Error detection in motor behavior is a fundamental cognitive function heavily relying on cortical information processing. Neuronal activity in the high-gamma frequency band (HGB) closely reflects such local cortical processing, but little is known about its role in error processing, particularly in the healthy human brain. Here we characterize the error-related response of the human brain based on data obtained with noninvasive EEG optimized for HGB mapping in 31 healthy subjects (15 females, 16 males), and additional intracranial EEG data from 9 epilepsy patients (4 females, 5 males). For the first time, our findings reveal a comprehensive picture of the global and local dynamics of error-related HGB activity in the human brain. On the global level as reflected in the noninvasive EEG, the error-related response started with an early component dominated by anterior brain regions, followed by a shift to parietal regions, and a subsequent phase characterized by sustained parietal HGB activity. This phase lasted for more than 1 s after the error onset. On the local level as reflected in the intracranial EEG, a cascade of both transient and sustained error-related responses involved an even more extended network, extending beyond frontal and parietal regions to the insula and hippocampus. HGB mapping appeared especially well suited to investigate late, sustained components of the error response, possibly linked to downstream functional stages such as error-related learning and behavioral adaptation. Our findings establish the basic spatio-temporal properties of HGB activity as a neuronal correlate of error processing, complementing traditional error-related potential studies.

Significance Statement

There is great interest to understand how the brain deals with errors in goal-directed behavior. An important index of cortical information processing is fast oscillatory brain activity, particularly in the high-gamma band (above 50 Hz). Here we show for the first time that it is possible to detect error-related high-gamma responses with noninvasive techniques, characterize these responses comprehensively, and validate the EEG procedure for the detection of such signals. In addition, we demonstrate the added value of intracranial recordings pinpointing the fine-grained spatio-temporal patterns in the error-related brain networks. We anticipate that the optimized noninvasive EEG techniques as described here will be helpful in many areas of cognitive neuroscience where fast oscillatory brain activity is of interest.

Introduction

Error processing is a fundamental brain function. A breakthrough in research on error processing in the human brain was the independent discovery of the “error-related negativity” (ERN) (Gehring et al., 1993), or error negativity (Ne) (Falkenstein et al., 1991) in noninvasive electroencephalography (EEG). The ERN/Ne is a negative deflection above the fronto-central midline, peaking shortly after the electromyogram (EMG) onset of an erroneous response, followed by the error positivity (Pe) (Falkenstein et al., 1991) with parietal maximum. ERN/Ne and Pe are often assumed to reflect sequential functional aspects of error processing, including precursors of error detection such as conflict monitoring and explicit error detection itself. In contrast to the ERN/Ne, the Pe was linked to conscious error processing (Nieuwenhuis et al., 2001). Moreover, the Pe might reflect

evidence strength during error detection and could thus provide input to further downstream stages, e.g., to the evaluation of the significance of errors and the implementation of behavioral consequences (Steinhauser and Yeung, 2010).

To further dissect error-related processing both in healthy subjects and in patients with a broad spectrum of brain disorders (Alain et al., 2002; Hajcak et al., 2003; Shiels and Hawk, 2010), subsequent studies increasingly utilized time-frequency decomposition of error-related EEG responses. These studies revealed spatial and dynamical behavior of lower frequency bands like delta, theta, alpha and beta (Table 1) unfolding alongside the time-domain (ERN/Ne & Pe) potential changes. There is only limited data on the role of higher frequencies in error processing, coming from intracranial recordings in neurological patients (Bastin et al., 2017) and to the best of our knowledge none from noninvasive EEG recorded from the healthy human brain.

However, gamma-band frequencies may be especially important to understand cortical function in general, including error processing. A large body of empirical evidence indicates that high-gamma band (HGB, including the 50-150 Hz range) activity is a spatially and temporally specific index of the underlying, functionally relevant neuronal networks (Crone et al., 1998, 2006; Brunel and Wang, 2003). Compared to lower frequencies, however, detecting HGB power modulations in noninvasive EEG is challenging for several reasons that are related to the more focal spatial distribution of cortical high-frequency sources (Crone et al., 2006), their much smaller power, (Freeman et al., 2000), and their greater susceptibility to artifacts, such as from muscle activity (Goncharova et al., 2003) or microsaccades. The latter particularly can mimic physiological responses within the HGB range (Yuval-Greenberg et al., 2008).

To overcome these problems, we carefully optimized the procedure of EEG acquisition and analysis for the detection of high-frequency EEG modulations, combining high-resolution EEG acquisition, optimized electromagnetic shielding, low-noise amplifier systems, as well as high-precision eye tracking simultaneously acquired to the EEG data to tightly control for ocular artifacts. Utilizing this optimized setup, we re-examined a classical paradigm to elicit error responses in a large group (n=35) of healthy subjects. Furthermore, to validate our noninvasive EEG findings, we also ran the same paradigm in patients with intracranially implanted electrodes.

Our findings clearly demonstrate that error-related HGB brain responses can be detected in noninvasive EEG recorded from healthy subjects; importantly, we rule out ocular including micro-saccadic effects as an explanation for the observed HGB responses, as well as corroborate our noninvasive observations by intracranial EEG data. For the first time, our findings reveal a clear picture of the global dynamics of the error-related HGB response of the human brain, starting from an early response dominated by anterior brain regions, over a shift to medial parietal regions parallel to the Pe potential, and finally to a subsequent phase characterized by sustained parietal HGB activity. This phase lasts for more than 1 s after the onset of the error event and constituting a novel candidate signal of the downstream processes following the classical Pe. Combined investigation of both the classical error-related potentials and of HGB modulations thus promises to shed new light on error processing in the human brain.

Materials & Methods

Subjects

In the noninvasive EEG study, 35 healthy subjects participated; thereof, 4 subjects had to be excluded because of extensive muscular or ocular artifacts. Thus, data of 31 subjects (mean age 24.6 years, standard deviation (SD) = 3.1 years, 15 females) were further analyzed. Handedness was assessed according to a modified Edinburgh handedness questionnaire (Oldfield, 1971); 28 subjects were right-handed, 3 were left-handed. All stated not to have neurological or psychiatric diseases and not to be under the influence of medication affecting the central nervous system.

In the intracranial EEG study, 9 right-handed patients (mean age 27.0 years, SD = 7.7 years, 4 females) with pharmacoresistant epilepsy participated. They were implanted with intracranial electrodes in Freiburg, Germany, or in Prague, Czech Republic.

All subjects and patients gave their written informed consent before participating in the study. The study was approved by the local ethics committees.

Experimental design

To probe error-related processing, we used the Eriksen flanker task (Eriksen and Eriksen, 1979) (Fig. 1) as employed in a pioneering study in this field of research (Gehring et al., 1993) as well as in many follow-up publications (Kopp et al., 1996; Botvinick et al., 1999; Gehring and Knight, 2000; Nieuwenhuis et al., 2002; Ridderinkhof et al., 2002; Herrmann et al., 2004b; Albrecht et al., 2009; Maier et al., 2012; Zavala et al., 2013). At the beginning of each trial, a cue in the form of an asterisk was shown to the subjects in the center of a 19-inch monitor (4:3-screen ratio, 60-Hz frame rate) for 1 s. After that, one of four stimuli

was shown for 100 ms, each with a probability of 0.25. Two of the stimuli were *congruent stimuli* (LLLLL & RRRRR) and the other two *incongruent stimuli* (RRLRR & LLRLL). To respond, subjects used their left or right index finger to press the left or right analog shoulder button on a wireless gamepad (Logitech F710, Apples, Switzerland) if the central letter of the stimulus was an “L” or "R", respectively. The deflection threshold of the analog joystick button was set to 10% of its maximal deflection.

As proposed by (Herrmann et al., 2004b), we set an individual reaction time limit for each subject. This response time limit was determined as the mean response time in a 32-trial training session. Subjects were instructed to respond as fast and accurately as possible. The subjects were also introduced to a scoring point system, and instructed to get as many points as possible. For each correct response, subjects gained 5 points, and lost 5 points in the event of an erroneous response. By missing the individual reaction time limit, subjects lost 10 points; this stronger penalty was introduced to keep the subject under time pressure, hence inducing errors. In each break after a recording run, the score and performance of the respective run was shown to the subjects along with a comparison to their total performance up to this run.

Two seconds after their response, the subjects received an audiovisual feedback according to their performance. If the response was fast enough and correct, the feedback consisted of a smiling face icon and a 1-kHz sine tone, which produced an encouraging impression; the feedback for an erroneous but fast enough response consisted of a sad face and a 500-Hz sine tone, which produced a less-encouraging impression. For responses slower than the individual reaction time limit, a cartoon of a snail was displayed accompanied by a 5-kHz sine tone, which produced a more unpleasant impression.

Before the start of each trial, only the fixation dot was shown for 3 s. In the case of healthy subjects, one session consisted of 100 trials, after which the subjects had the possibility to have a break. Each experiment included 10 sessions, so that altogether 1000 trials were collected for each subject. Recording sessions with epilepsy patients were shorter and included overall fewer trials depending on the condition of the respective patient. In average, patients completed 369 ± 111 (mean ± SD) trials.

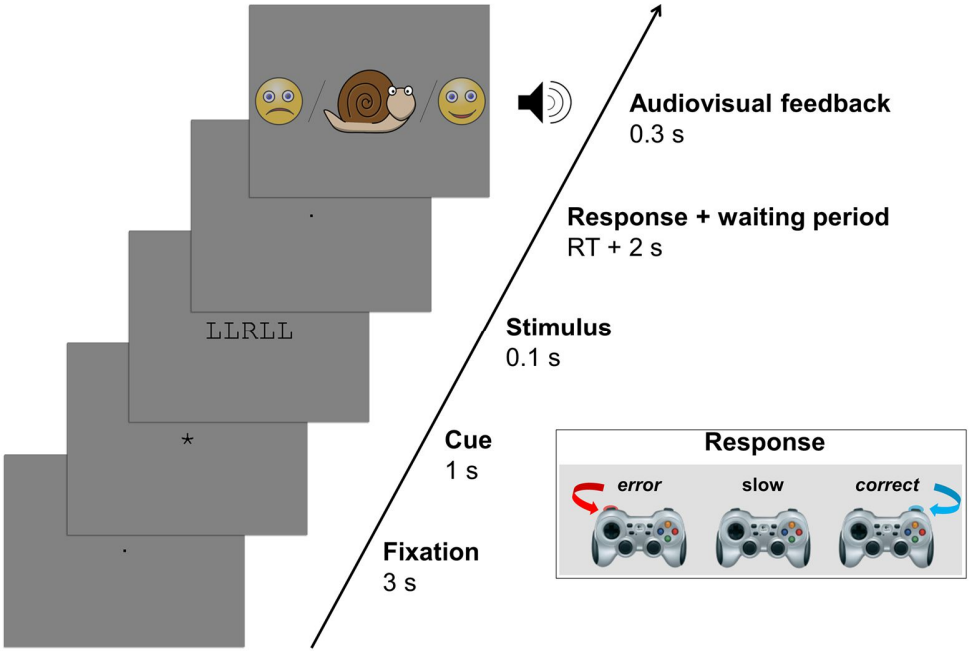

Figure 1: Flowchart of the Eriksen flanker task paradigm used to elicit errors.

After a fixation period (3 s), and a cue period (1 s), the stimulus appeared for a short period of time (100 ms). Subjects had only a limited amount of time, individually set to their reaction time (RT) in a familiarization phase of the experiment, to press a gamepad button with their left index finger if the central letter of the stimulus was an “L” or with their right index finger if the central letter was an “R” (see inset). 2 s after the button press, one of the three types of audiovisual feedback indicated to the subjects whether their response was correct, incorrect, or too slow.

Recording and preprocessing of noninvasive EEG

The noninvasive EEG setup was optimized for the measurement of high-frequency responses. We used NeurOne amplifiers (Mega Electronics Ltd., Kuopio, Finland) with a 24-bit resolution and low input noise (root mean square < 0.6 µV between 0.16-200 Hz). We recorded 128 EEG channels with the waveguard EEG cap (ANT Neuro, Enschede, Netherlands) with a sampling rate of 5 kHz (AC, 1250-Hz anti-aliasing low-pass filter). The cap held sintered Ag/AgCl electrode elements and was available in three different sizes to be suitable for variable head sizes. Electrode position Cz was used as recording reference; the ground was located between AFz and Fz. Whenever possible, impedances were kept below 5 kΩ. Additional measurements included electrooculography (EOG) with 4 electrodes around the eyes, 2-channel electrocardiography (ECG) and bipolar electromyography (EMG) above the forearm flexor muscles of both arms and above the gastrocnemius muscle of both legs; EMG, EOG and ECG were recorded with self-adhesive electrodes.

The EEG recordings took place in an electromagnetically shielded cabin ("mrShield" - CFW Trading Ltd, Heiden, Switzerland) to reduce electromagnetic artifact contamination. All exchange of information between inside and outside of the cabin was done with fiber optic cables to sustain the shielding. Also, electrical devices inside the cabin, such as EEG amplifier, eye tracker and loudspeakers, were powered by DC batteries to prevent 50-Hz power line artifacts from interfering with the EEG signal. The cabin furthermore dampens sounds and vibrations to protect the subject from external noise.

Both control of the experiment as well as data analysis was carried out using Matlab R2014a (The MathWorks Inc., Natick, USA, RRID:SCR_001622). Implementation of the

paradigm was done within the Psychophysics Toolbox (Brainard, 1997, RRID:SCR_002881). Synchronization of the EEG data and the experimental paradigm was achieved by using a parallel port to send different trigger pulses for each event from Matlab to the EEG amplifiers.

To control the signal quality, a visual inspection of the EEG data was done both continuously during the measurement as well as after the experiment in Brainstorm (Tadel et al., 2011). We searched for EMG artifacts by examining time course and topography of single-trial data. Channels with strong contamination with EMG artifacts were excluded from further analysis in single subjects; on average, we rejected 1.03 ± 1.75 (mean ± SD) channels.

During signal processing, the EEG data and markers were down-sampled from 5 kHz to 500 Hz. Channels were re-referenced to their common average. The signal was filtered with a Butterworth high-pass filter of fourth order with a cut-off frequency of 0.5 Hz.

The indices of the correct and false responses were extracted and aligned on the response EMG. The time point of the EMG onset was found by applying a threshold based retrospective search on the arm EMG channels.

Intracranial EEG recording, localization and preprocessing

Recording of intracranial EEG signal was done either with Compumedics amplifiers (Singen, Germany) at the epilepsy center in Freiburg, Germany (2 kHz sampling rate), or with Schwarzer Epas amplifiers (Munich, Germany) and Nicolet EEG C-series amplifiers (Pleasanton, USA) at the epilepsy center of the Motol University Hospital in Prague, Czech Republic (512 Hz sampling rate). The depth electrodes used for recording had platinum-

iridium contacts (DIXI Medical, Lyon, France & AD-TECH, Racine, WI, USA).

The preprocessing was done as for the noninvasive data, with the difference that the channels were re-referenced bipolarly between the respective neighbors.

The stereotactic depth electrodes were localized with the help of their post-implantation MRI or CT artifacts in a normalized and co-registered MRI of each patient as described in Pistohl et al. (2012). After transformation to the MNI coordinate system, cytoarchitectonic probabilistic maps were calculated with the SPM anatomy toolbox (Eickhoff et al., 2005, 2006, 2007) to assign the electrodes to specific brain regions. This method accounts for inter-subject differences in brain anatomy and allows the comparison on a group level with high precision (Amunts et al., 2007).

Electrodes positioned inside a seizure onset zone or showing frequent interictal activity, as identified by experienced epileptologists, were excluded from further analysis. Of 885 bipolar referenced channels from 9 patients, we removed 76 channels because they could not be assigned to a specific brain region, 53 channels which were positioned inside a seizure onset zone, 59 channels because of frequent interictal activity, and 7 channels due to technical problems or position outside the brain. Thus, 690 sites were available for further analysis.

The visualization of intracranial and scalp EEG electrodes in relation to the cortex surface was done with Brainstorm (Tadel et al., 2011). The intracranial electrodes were visualized on an ICBM152 brain template (Mazziotta et al., 2001; Fonov et al., 2009).

Time-frequency analysis

Time-resolved spectral power was computed with a multitaper method (Thomson, 1982) with a window length of 500 ms, a step size of 50 ms and two Slepian taper functions. Trial averages were computed with a median function to exclude outliers. To visualize error-related power modulations we baselined all time-frequency bins in each error trial by the corresponding bin of the median correct response trial (i.e. by dividing the error responses by median of the correct responses). Thus, the motor-related activity common to both response types canceled out. For calculation of error-related activity or power, this method of baselining was applied.

Exclusion and statistical matching of ocular artifacts

Ocular movements were recorded with the EyeLink 1000 plus (SR Research Ltd., Ottawa, Canada, RRID:SCR_009602), enabling binocular eye movement recordings with a high-speed infrared illuminator and camera; the sampling rate for binocular recording was 500 Hz.

For the extraction of microsaccades, an algorithm as described by Engbert and Kliegl (2003) was used with the default minimal microsaccade duration threshold of 12 ms. Time points of blinks and saccades were identified with the algorithms provided by the EyeLink recording software.

All trials in which a blink occurred within the time window of 0.5 s prior and 2 s after the response were excluded from further analysis to ensure that the EEG signal in the analyzed time frame was not contaminated with blink artifacts.

To exclude possible influences of saccades and microsaccades on high-frequency EEG correlates, we matched each time bin of the correct and error trials after the time frequency decomposition. This was done by incrementally removing time bins from the correct condition, which always had more trials. At each iteration step, the time bin which contributed the most to the residual difference, as calculated by a sum of squares of saccade and microsaccade counts, was removed. This process was repeated until the p-value calculated with a sign test comparing error and correct condition was greater than 0.3.

Statistical analysis

For visualization of median voltage, the standard error of the median was calculated per condition using bootstrap sampling (Moore and McCabe, 1989) with 1000 re-samples, using the 2.5^{th} and 97.5^{th} percentile of the population as standard error. Median time or frequency bins which had a significant difference between the correct and erroneous condition were identified with the Wilcoxon rank sum test (Mann and Whitney, 1947). Significance of median power changes within individual conditions was computed with a two-sided sign test (Dixon and Mood, 1946). P-values were corrected for multiple testing by false discovery rate (FDR) correction (Benjamini and Hochberg, 1995).

Results

Here we show for the first-time error-related high-gamma responses in a noninvasive EEG study (with 31 healthy subjects) and additionally compare and corroborate them with intracranial EEG measurements (in 9 patients with pharmacoresistant epilepsy).

Error-related voltage and spectral power modulations in noninvasive EEG

Error-related voltage and spectral power modulations in surface EEG, as averaged over the 31 healthy subjects included in this study, are shown in Fig. 2. Topography and time course of the classical ERN/Ne and Pe components can be seen in the upper part. In the lower part of the figure, the relative power differences between error and correct condition are plotted in four frequency ranges at the time point of the ERN/Ne and Pe components. The black outlines in Fig. B and C show the area where the ERN/Ne and the Pe components were significant with $p<0.01$ at their respective maxima.

The high-gamma band response, shown here for the time window between 70 and 80 Hz, exhibited significantly higher power in error than correct responses. In the time window of the ERN/Ne maximum, the error-related HGB power was centered at fronto-central channels, while it started to relocate into more posterior areas at the maximum of the Pe.

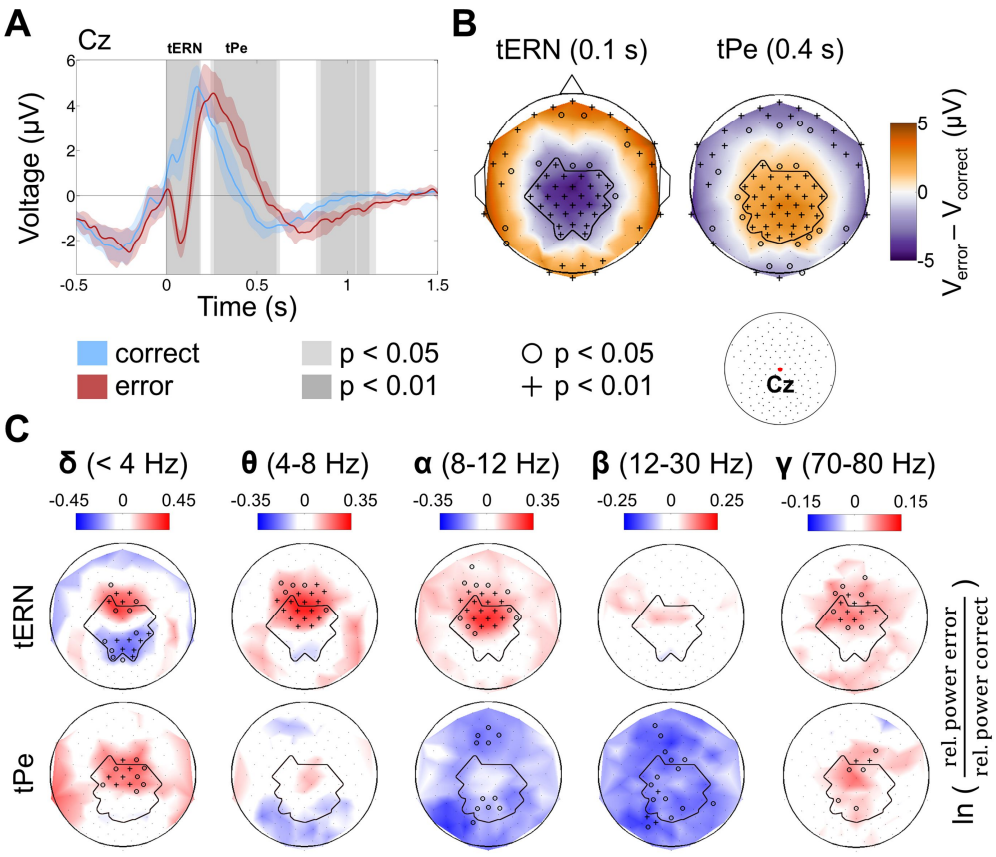

Figure 2: Error-related voltage and spectral power modulations in high-density EEG.

A) Single channel plot (electrode position Cz) locked to response EMG onset. The median correct response is shown in blue, the median erroneous response in red. The standard error of the median is plotted semitransparent. The vertical dotted line marks the EMG onset. Times with significant differences between the error and correct condition are shown with a gray background. **B)** Topographical map of the event-related potentials at the time of the ERN/Ne (t_{ERN}) and the Pe (t_{Pe}) components. Median voltage difference between error and correct trials is shown color coded. Electrodes with significant differences are marked with “o” or “+” (Wilcoxon rank sum test, FDR-corrected, $p<0.05$ or $p<0.01$, respectively). **C)** Error-related spectral power modulations in the theta, alpha, beta, and high-gamma range. Logarithmic relative power of the median erroneous response baselined with median correct response is shown color coded. Significant sites as determined (FDR-corrected sign test) are marked as in (B). Error-related effects in the high-gamma range had a maximum at fronto-central sites at the time of the ERN/Ne peak; at the time of the Pe maximum, the HGB increase was shifted to midline electrodes in a parietal direction.

A broader overview of the dynamics and topography of error-related voltage and spectral power modulations is shown in Fig. 3, with error-related spectral power responses up to 120 Hz in the time interval from 0.2 s before until 1.5 s after the response.

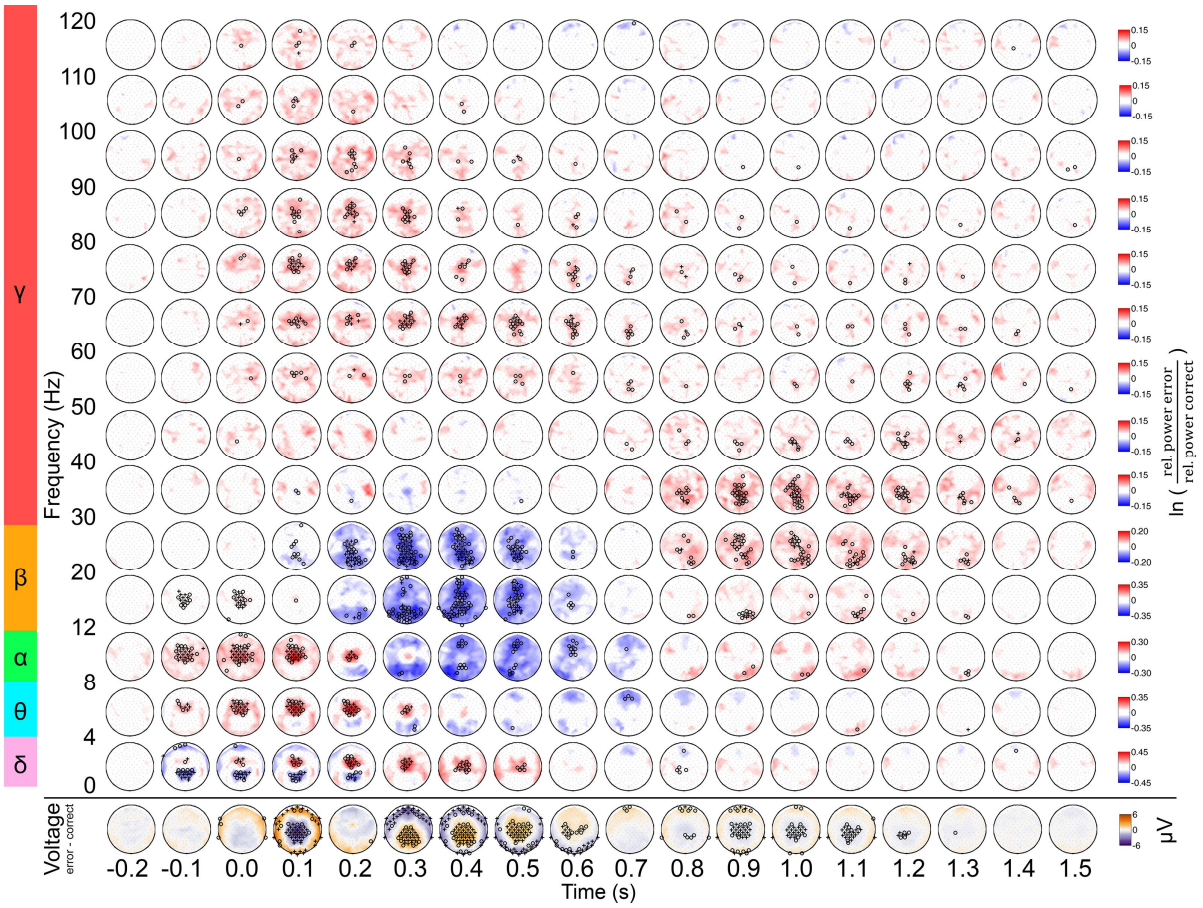

Figure 3: Topography of error-related voltage and spectral power modulations.

The circular plots represent a top view of the head with the nose pointing up. At the bottom, voltage differences between error and correct response are shown topographically (median of 31 subjects). Above, median error-related spectral power modulations are depicted for 14 frequency bands from 0 to 120 Hz. Red color indicates higher power in error responses, while blue color indicates higher power in correct responses. Electrodes with significant differences between error and correct condition are marked as in Fig. 2 B. The data is aligned to response onset.

Comparing error and correct conditions, significant differences became evident. While there was lower power at parietal channels in the delta band (< 4 Hz) during and after

errors, fronto-central channels exhibited an error-related power increase in the delta and the theta band (4-8 Hz). In the alpha band (8-12 Hz), a spatially more widespread power increase during and shortly after the erroneous response occurred, followed by an attenuation with lower power compared to correct responses. Within the beta band (12-30 Hz), a widespread power decrease concurred with the Pe. In the low-gamma band (LGB, 30-50 Hz), differences were mostly apparent at a later time, starting 800 ms post-response in the form of a power increase in the 30-40 Hz frequency range. Simultaneously with the late LGB increase, a second (with the ERN/Ne being the first) significant negative voltage deflection was seen at central channels.

Crucial to the present study, in the high-gamma band (HGB, > 50 Hz), a significant error-related power increase occurred at fronto-central channels shortly after the response onset, and shifted to more central and parietal areas over the course of a few hundred milliseconds, where the error-vs-correct relative HGB power stayed significantly increased until up to 1.5 s after the response. The frequency profile of the HGB response showed a maximum between 60 and 90 Hz. Similar high-gamma increases were observed in errors both after incongruent and congruent stimuli classes (data not shown).

We calculated Spearman's rank correlation level between the ERN/Ne and Pe amplitude and the error-related spectral modulations in the 70-80 Hz band across subjects. The calculation was done on the signals of the channels with the maximal amplitudes of the components of interest, which was FCz for the ERN/Ne and CPz for the Pe component. There was no significant correlation found. Spearman’s rho for the ERN/Ne with error-related HGB components was $r_s = -0.05$ and $p = 0.78$, and for Pe $r_s = 0.10$ and $p = 0.58$.

Effects of eye movements on high-gamma signals

During the experiments, a great number of miniature eye movements were recorded for each subject. After discarding those events near blinks, per subject on average 6300 ± 2500 (mean ± SD) microsaccades were accumulated. To examine the spectral power modulations related to this class of eye movements more closely, we also examined EEG data aligned to the onset of the microsaccades. Fig. 4 shows the group median of those trials. Both at fronto-polar and parieto-central EEG channels, there was a broad-band gamma increase during microsaccade (and saccade, data not shown) onset. This increase was prominent from 25 to 120 Hz. In lower frequency bands, e.g., in the delta band, we observed a power decrease, which continued until 500 to 600 ms after the microsaccade onset.

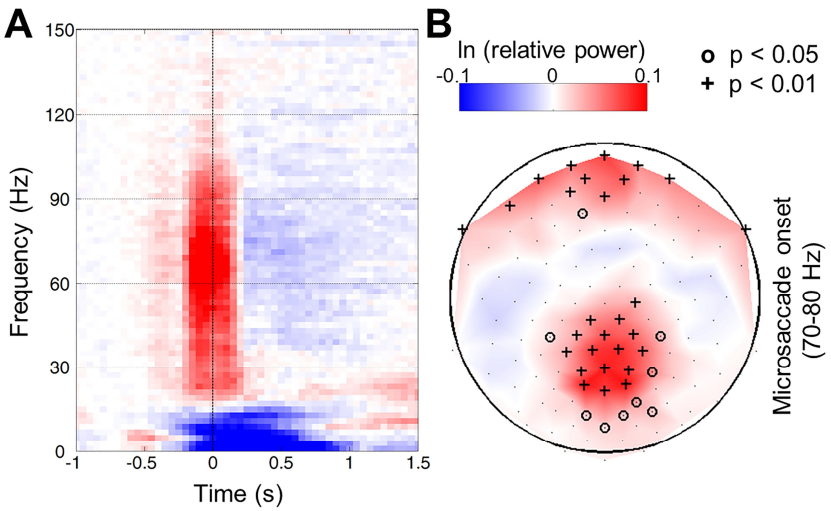

Figure 4: Microsaccade-related time-frequency spectrum in scalp EEG.

The plots show a group median of the 31 subjects; the data is aligned to microsaccade onset. **A)** Time-frequency plot of a parieto-central channel (Pz). The log-power (color-coded) was taken relative to a baseline from -1 s to –0.5 s. **B)** Topography of 70-80 Hz high-gamma relative power at the time of microsaccade onset. Electrodes with significant differences are marked with “o” or “+” (sign test, FDR-corrected, $p<0.05$ and $p<0.01$, respectively).

Next, in each subject we matched the correct and error condition to have the same amount of microsaccades and saccades within each time-frequency bin of the EEG data after the multitaper analysis. To examine the effect of this measure on the results, we compared the error-related high-gamma activity in matched and unmatched data (Fig. 5).

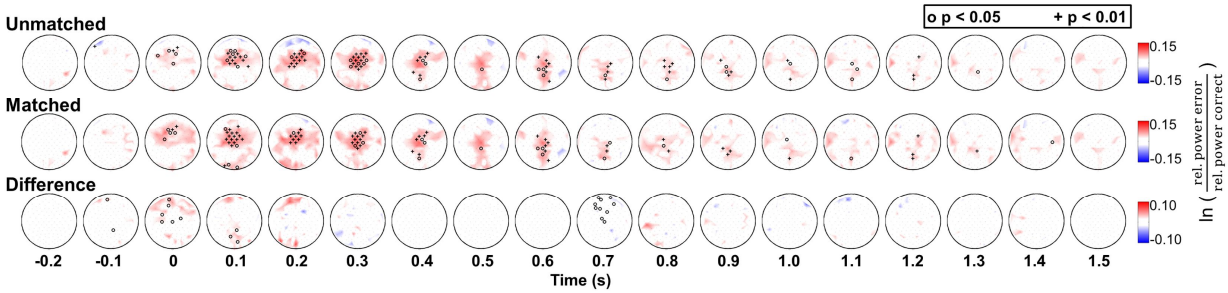

Figure 5: Influence of saccade and microsaccade matching on error-related high-gamma in noninvasive EEG. All plots show group results of the 31 subjects, aligned to EMG response onset. In the top row, error-related high-gamma activity in the 70-80 Hz range is plotted for the data before matching. The middle row depicts the same results after matching each time bin for microsaccade and saccade frequency. In the bottom row, the differences between unmatched and matched data are shown. Significant sites are marked as in Fig. 4.

After the matching, the distribution of electrodes with significant changes in the high-gamma band was only minimally altered, and the overall pattern remained the same. There were only very few significant differences between the original and the matched data. We conclude the error-related effects cannot be attributed to the occurrence of saccades and microsaccades.

Error-related high-gamma activity: frontal vs. parietal regions

We further wished to compare error-related high-gamma activity at frontal and parietal regions as the two major foci of the HGB response. To this aim, we averaged HGB activity in a frontal and a parietal region of interest (ROI).

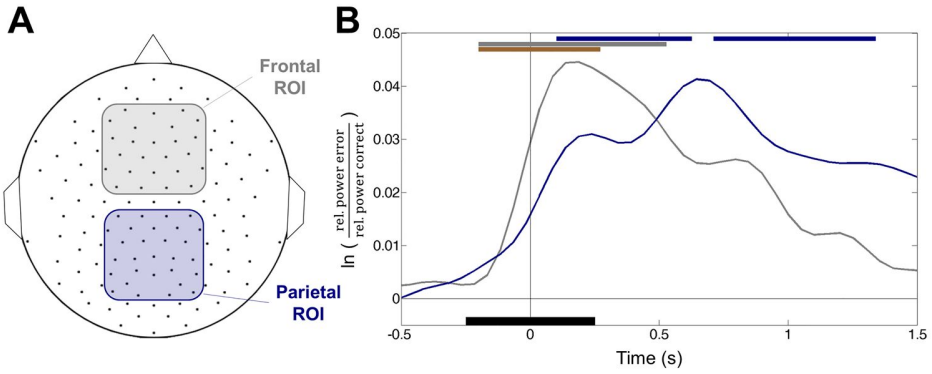

Figure 6: Time course of error-related 70-80 Hz HGB activity in frontal and parietal regions.

A) Illustration of the frontal region of interest (ROI) including 25 electrodes (gray) and a parietal ROI with 27 electrodes (blue). **B)** The median error-related 70-80 Hz high-gamma power is plotted for both ROIs in the respective colors. The bars above indicate times when the HGB activity in the frontal (gray), parietal (blue) or difference of both ROIs (brown) was significant (sign test, $p<0.01$). Time point zero represents the response EMG onset. The black bar around 0 s at the bottom of the plot indicates the temporal width of the Gaussian window function (0.5 s) used for the time-resolved spectral density estimation during moving average-calculation, explaining the smoothness of the curves above.

Error-related HGB power in the frontal ROI reached its maximum around 150 to 200 ms after response EMG response onset. The same frequency band in the parietal ROI showed a later peak at 600 to 700 ms. The HGB power in the parietal ROI was significantly increased until up to 1.3 s after the EMG response onset. In the time around the EMG onset, error-related HGB activity in the frontal ROI was significantly (sign test, $p<0.01$) stronger than in parietal regions.

Confirmation in Intracranial EEG Measurements

Intracranial EEG measurements in 9 patients yielded a multitude of error-related changes. For comparability, we concentrated the analysis of error-related high-gamma activity in intracranial EEG to the 70-80 Hz band, which had the strongest HGB activity in

noninvasive EEG. An overview of the electrode locations of all 9 patients and sites with significant changes in 70-80 Hz high-gamma activity after errors is shown in Fig. 7 together with examples of single-channel time-frequency responses.

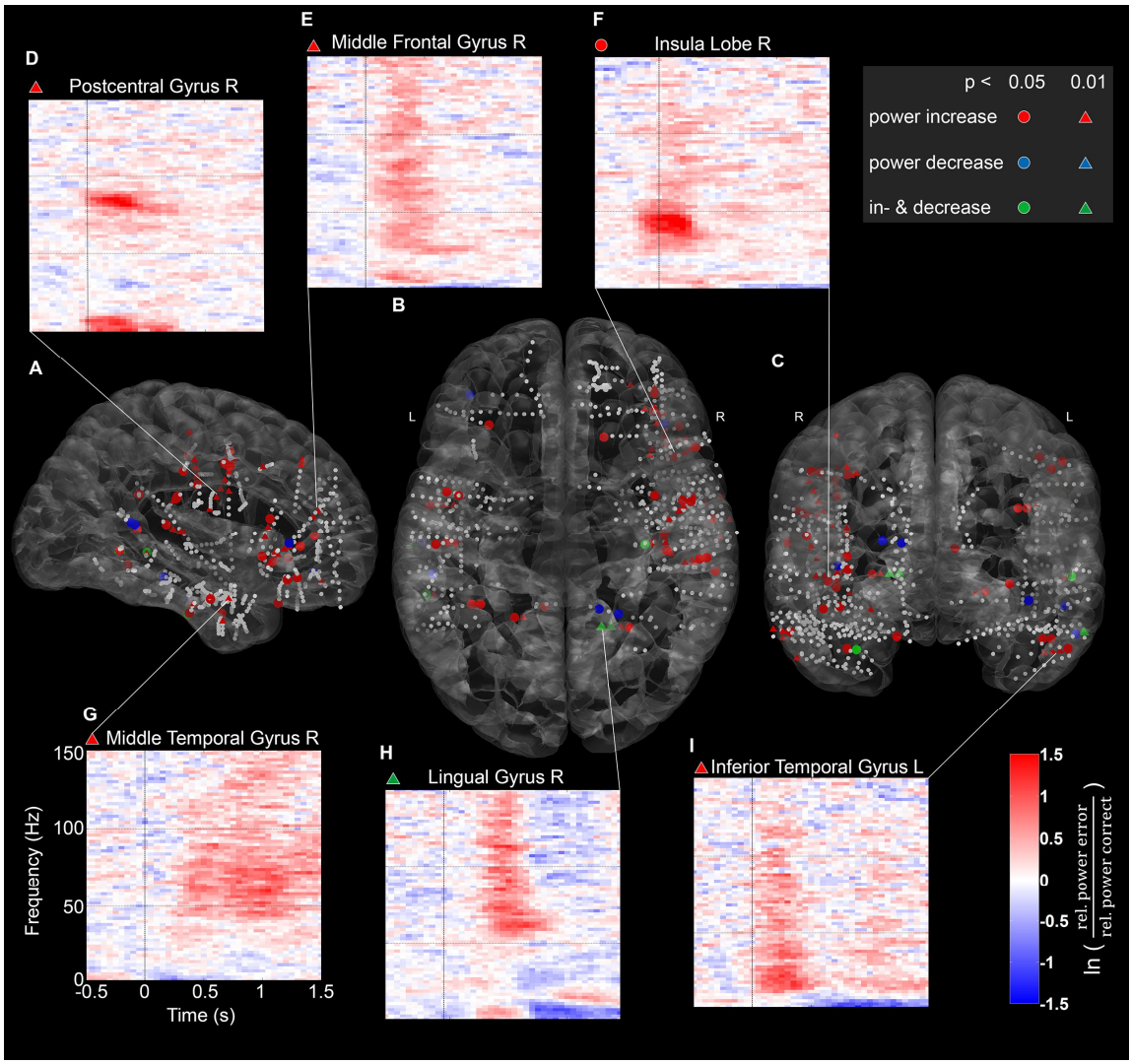

Figure 7: Error-related high-gamma (70-80 Hz) responses in intracranial EEG.

Depth electrodes of 9 epilepsy patients are plotted in white on the semi-transparent ICBM152 brain template from sagittal (A), axial (B), and coronal (C) views. Sites with significant activations in the 70-80 Hz range were marked with colored circles or triangles (sign test, FDR-corrected, $p<0.05$ or $p<0.01$). The marker color indicates whether there was a significant increase (red), decrease (blue), or both (green) in a time window from 0-2 s relative to the response. Exemplary single-channel time-frequency plots are shown above and below together with their assignment to anatomical areas. Color scale as in Fig. 2 C.

We found error-related high-gamma modulations in multiple areas. The areas with evidence of increased 70-80 Hz high-gamma error-related power from two or more independent patients were all in the right hemisphere, namely the insula, the superior orbital gyrus, the inferior frontal gyrus, the middle frontal gyrus, and the precentral as well as the postcentral gyri. It is also to note that our sample consisted of more electrodes in the right hemisphere (443 sites after bipolar re-referencing & channel rejection) compared to the left hemisphere (247 sites). Other areas in single patients with multiple electrode sites with significant HGB changes included the right transverse temporal gyri, the right supramarginal gyrus, the right precuneus, the right and left middle temporal gyrus, the left inferior temporal gyrus, the left precentral gyrus, and the right and left lingual gyrus. Decreased high-gamma activity after errors was found in the left inferior frontal gyrus, the right precuneus, the left inferior temporal gyrus, and the right lingual gyrus.

As is noticeable in the exemplary time-frequency plots, there are different types of error-related HGB modulations in intracranial EEG. First, there are areas where the HGB power increase shows a clear maximum and is restricted to a small area in time and frequency, as the postcentral gyrus and the insula (Fig. 7 D,F). Second, there are examples like the middle frontal gyrus, the lingual gyrus or the inferior temporal gyrus (Fig. 7 E,H,I) with a broadband gamma increase which was temporally transient. Third, a broad-band gamma increase with a long duration of 2 s was observed in the middle temporal gyrus (Fig. 7 G).

We further compared error-related spectral power modulations of nearby intracranial EEG and scalp EEG electrodes in the range of the motor cortex (Fig. 8).

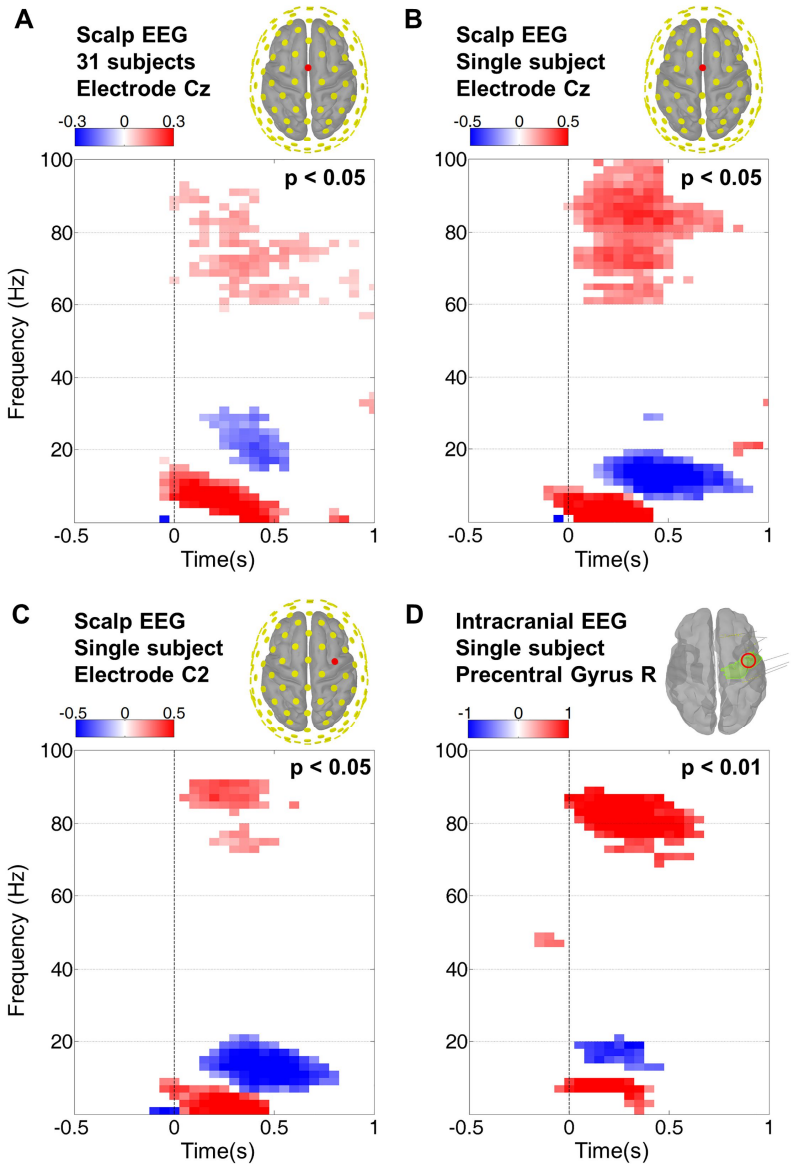

Figure 8: Comparison of intracranial EEG with scalp EEG in group and single subject results.

The color scale depicts the logarithmic relative power of the median error-related response baselined with the correct response. Only significant power modulations are shown with the threshold as labeled in the top right corner of the respective plot. Calculation of p-values was done with an FDR-corrected Wilcoxon rank sum test (single subjects) and an FDR-corrected sign test (group results). **A)** Group median (31 subjects) of error-related spectral power modulations at electrode Cz. **B)** Single-subject error-related spectral power modulations in EEG at electrode Cz. **C)** Single-subject error-related spectral power modulations in EEG at electrode C2. **D)** Single-subject error-related spectral power modulations in intracranial EEG within the right precentral gyrus in close proximity of the C2 electrode standard position.

Both in scalp EEG and intracranial EEG, significant error-related power modulations were observed in the delta, theta, alpha, beta, and high-gamma band. The spectral patterns of nearby intracranial and noninvasive EEG channels were very similar at both group and single-subject level (Fig. 8). In intracranial EEG, the high-gamma activity had the strongest error-specific power modulation, while in noninvasive measurements, the lower frequency bands showed a greater difference between correct and error responses.

Fine-grained dynamics of error-related activity in intracranial EEG

For a closer look at the spatio-temporal progression of error-related activity across the brain, we analyzed significant in- and decreases of error-related low- and high-spectral power in the intracranial recorded data of all 9 patients (Fig. 9).

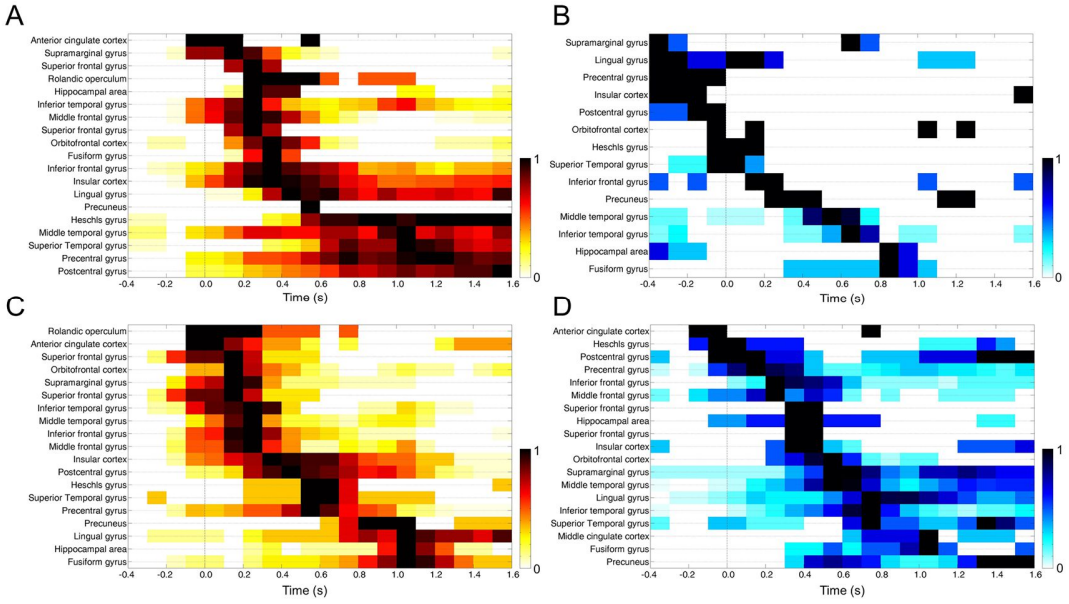

Figure 9: Time course of significant error-related power in- and decreases in intracranial EEG.

For each area, the total number of significant increases (red) and decreases (blue) in all patients were normalized; the areas were sorted according to the time with the maximal count (equal to 1) in ascending order. Time course of HGB power modulations in the range 50-120 Hz are shown at the top (A, B), low-frequency components below 30 Hz are shown at the bottom (C, D). The data is aligned to response onset.

It is apparent that low and high frequencies, as well as power increases and decreases, differed in their spatial distribution over time. Subareas in frontal, temporal, and parietal brain regions were activated at various time points before, during and after the error response. Error-related increases in the high-gamma range (Fig. 9 A) especially exhibited a temporal development that started at frontal surface und deep areas, including the ACC, and then advanced to both parietal and temporal regions of the brain. Notably, increased error-related HGB activity in hippocampal areas peaked 0.3 s after the response, while decreased hippocampal HGB activity (Fig. 9 B) occurred -0.4 to -0.2 s before the response and again 0.8 to 1.0 s after the response. Overall, intracranial EEG portrays a consistent but much more complex picture of error processing compared to noninvasive data.

Discussion

Converging evidence indicates an important role of HGB activity in cortical function (Başar et al., 2001; Herrmann et al., 2004a; Fries, 2005; Canolty et al., 2006; Crone et al., 2006; Jensen et al., 2007; Buzsáki and Wang, 2012) Beyond studies investigating passive sensory stimulation, however, only relatively few studies so far succeeded to demonstrate HGB activity related to active behavior in noninvasive EEG (Shibata et al., 1999; Ball et al., 2008; Darvas et al., 2010; Nottage et al., 2013; Smith et al., 2014). In the present study, we examined error processing in the human brain as reflected in HGB activity, based on measurements using noninvasive and intracranial EEG. In both, we found significant error-related modulations of high-gamma power. Noninvasive 128-channel EEG in an electromagnetically shielded cabin enabled us to reveal the global topography and dynamics of event-related potentials and spectral power modulations, while we used

intracranial EEG to validate the noninvasive findings, and additionally to probe local fine-grained activity patterns.

Error-related low-frequency responses in noninvasive EEG

Our findings generally reproduced the spectral power modulations in the delta, theta, alpha and beta bands in noninvasive EEG as reported by previous studies (Luu et al., 2004; Yordanova et al., 2004; Kolev et al., 2005; Trujillo and Allen, 2007; Koelewijn et al., 2008; Carp and Compton, 2009). Further, our results also revealed several unreported topographical features.

For example, we observed an error-related delta band pattern characterized by the co-occurrence of increased and decreased power in anterior and posterior regions, respectively (Fig. 2,3). In the high-beta and low-gamma band (20 - 40 Hz), we observed an error-related power increase in a late time window, starting 800 ms after the response (Fig. 3). Interestingly, around 1000 ms after response onset, a second (with the ERN/Ne being the first) smaller but significant ($p<0.01$) negative deflection in the error-related potential occurred at midline EEG channels (Fig. 3, bottom row) which thus might be termed “Ne1000”. The maximal low-gamma band response occurred at roughly the same time with a focus on midline channels. Together, these examples illustrate that an optimized EEG procedure applied to a suitably large group of subjects can reveal a range of additional significant features of the error-related response that may be useful to consider in future studies.

Error-related high-frequency responses in noninvasive EEG

Both in group results and single subjects, we found significant error-related HGB power

increases. Although high-gamma activity was seen in both correct and erroneous trials, it was significantly stronger in the erroneous trials. The error-related high-gamma response presented itself as an early fronto-central power increase, followed by a shift to parieto-central areas, where the HGB power stayed significantly above baseline levels over an extended period (up to 1.5 s, see Fig. 3,6) Importantly. the spatio-temporal dynamics differed clearly from those of theta, alpha, beta, and low-gamma responses, and high-gamma response were not correlated to ERN/Ne and Pe amplitudes across subjects, pointing to a unique functional role.

We controlled thoroughly for ocular artifacts in our noninvasive EEG experiments. Firstly, by using high-resolution binocular eye tracking, we were able to exactly match each time bin of the error-related and non-error-related time-frequency-resolved data for both microsaccade and saccade frequency and thus avoid a differential effect of ocular potentials (Yuval-Greenberg et al., 2008) on the error-related high-gamma signals. Secondly, the topography of microsaccade-related HGB effects showed a qualitatively different spatial pattern compared to the error-related HGB responses (Fig. 4, 5). Thus, we conclude that our error-related HGB responses cannot be explained as ocular artifacts.

Further, we also think that it is highly unlikely that our error-related HGB responses reflect EMG contamination. First, the error-related HGB power did not exhibit the rather flat, broadband power increase typical of EMG contamination (Goncharova et al., 2003), but rather a strong maximum between 60 and 90 Hz. Second, the spatial distribution of the high-gamma increase with the maximum over the midline was strikingly different from that to be expected for EMG, which has its emphasis on peripheral electrodes close to the muscles (Goncharova et al., 2003; Whitham et al., 2007).

Error-related high-gamma responses in intracranial EEG

Error-related intracranial high-gamma activity was found at multiple locations in the brain, showing much larger amplitudes than the extracranial counterparts. These areas overlapped strongly with areas where intracranial error-related potentials and HGB increases were previously reported (Brázdil et al., 2005; Bastin et al., 2017). In addition to gamma increases, we also observed responses with a decreased relative high-gamma power in relation to errors. They often followed a HGB power increase, possibly representing a systematic suppression aftereffect. As saccadic artifacts in intracranial EEG are mainly limited to the temporal pole (Jerbi et al., 2009), our intracranially recorded error-related HGB increases together with the results reported in 6 patients by Bastin et al. (2017) clearly show the existence of such responses on the cortex. Furthermore, as illustrated by Fig. 8, intracranial and scalp EEG channels placed above comparable brain regions showed strikingly similar time-frequency patterns in their error-related responses (see Fig. 8). Together, these observations lend additional support to the validity of our noninvasive data.

The time course of intracranial activations (Fig. 9) confirmed that frontal regions were activated rather early, while parietal (as well as temporal) areas became active later, in line with a downstream role in error processing. Intracranial data also clearly showed that, expectedly, cortical error processing is more complex than what can be observed in noninvasive EEG. Hippocampal high-gamma was significantly decreased prior to the actual error, and increased after the error. This could signify an interaction of error and memory systems, consistent with a role of gamma in memory functions (Howard et al., 2003; Kucewicz et al., 2017). Furthermore, Fig. 9 also demonstrates that lower HGB

power in pre-, postcentral, and supramarginal gyri as well as the insular cortex may precede errors. One explanation for that could be that high-gamma power could indicate a pre-activation or "readiness" of a brain area.

Potential functional relevance of HGB activity

Processing of behavioral errors involves several prominent sub-processes. These range from precursors of error detection, such as the evaluation of actual and intended action outcomes, including perceptual evidence accumulation, over the explicit error detection itself, to the evaluation of error importance, error-related learning, and behavioral adjustment (Holroyd and Coles, 2002; Carbonnell and Falkenstein, 2006; Taylor et al., 2007). Much research so far has focused on how these processes relate to the ERN/Ne and Pe complex. Recent evidence, based on systematic reward manipulations that targeted the criterion which participants used to decide whether or not to report errors, has linked the Pe to the strength of accumulated error-related evidence (Steinhauser and Yeung, 2010). This hints to the intriguing possibility that cognitive reactions to errors detection would be most likely reflected in brain signals occurring *after* the Pe. Our findings reveal sustained, significant HGB activity over the parietal cortex that substantially outlasted the duration of the Pe, up to at least 1.5 s after response onset. This timing would fit very well to high-level, late stage cognitive consequences of the detection of behavioral errors. The discovery of sustained error-related HGB activity thus may enrich future studies striving for a better sub-process-level understanding of the neuronal underpinnings of error processing in the human brain.

Conclusion & Outlook

The fact that error-related HGB signals are detectable with noninvasive EEG opens up a much wider avenue of research than would be feasible with intracranial recordings alone, particularly in healthy subjects and also in populations of patients with different neurological and psychiatric disorders, such as social phobias, autism spectrum disorders, schizophrenia, depression, as well as obsessive-compulsive disorder – all of which have been connected with alterations in the neuronal response to behavioral errors. Implantation of intracranial electrodes is however confined to a much smaller group of patients undergoing pre-neurosurgical evaluation, in most cases for the treatment of focal pharmacoresistant epilepsy. Our findings however clearly highlight the unique value of these intracranial recordings. For example, they allow assessment of brain structures that are difficult or even impossible to probe electrophysiological noninvasively, such as insular cortex and the hippocampal formation.

Our findings could help understanding the mechanisms behind human error processing. Further, they could also help in the decoding of errors from single-trial EEG using machine learning algorithms to improve the performance of brain-machine interfacing (Ferrez and Millan, 2008; Kreilinger et al., 2012; Spüler et al., 2012; Milekovic et al., 2013). More generally, we suggest that parallel investigations of error processing with both noninvasive as well as invasive recordings, and with attention to both classical error-related potentials as well as high-frequency signatures of error processing, might prove as the most fruitful way towards understanding the neural basis of this fundamental facet of cognition.

References

Alain C, McNeely HE, He Y, Christensen BK, West R (2002) Neurophysiological Evidence of Error-monitoring Deficits in Patients with Schizophrenia. Cereb Cortex 12:840–846.

Albrecht B, Heinrich H, Brandeis D, Uebel H, Yordanova J, Kolev V, Rothenberger A, Banaschewski T (2009) Flanker-Task in Children. J Psychophysiol 23:183–190.

Amunts K, Schleicher A, Zilles K (2007) Cytoarchitecture of the cerebral cortex—More than localization. NeuroImage 37:1061–1065.

Ball T, Demandt E, Mutschler I, Neitzel E, Mehring C, Vogt K, Aertsen A, Schulze-Bonhage A (2008) Movement related activity in the high gamma range of the human EEG. NeuroImage 41:302–310.

Başar E, Başar-Eroglu C, Karakaş S, Schürmann M (2001) Gamma, alpha, delta, and theta oscillations govern cognitive processes. Int J Psychophysiol 39:241–248.

Bastin J, Deman P, David O, Gueguen M, Benis D, Minotti L, Hoffman D, Combrisson E, Kujala J, Perrone-Bertolotti M, Kahane P, Lachaux J-P, Jerbi K (2017) Direct Recordings from Human Anterior Insula Reveal its Leading Role within the Error-Monitoring Network. Cereb Cortex 27:1545–1557.

Benjamini Y, Hochberg Y (1995) Controlling the False Discovery Rate: A Practical and Powerful Approach to Multiple Testing. J R Stat Soc Ser B Methodol 57:289–300.

Botvinick M, Nystrom LE, Fissell K, Carter CS, Cohen JD (1999) Conflict monitoring versus selection-for-action in anterior cingulate cortex. Nature 402:179–181.

Brainard DH (1997) The psychophysics toolbox. Spat Vis 10:433–436.

Brázdil M, Roman R, Daniel P, Rektor I (2005) Intracerebral Error-Related Negativity in a Simple Go/NoGo Task. J Psychophysiol 19:244–255.

Brunel N, Wang X-J (2003) What Determines the Frequency of Fast Network Oscillations With Irregular Neural Discharges? I. Synaptic Dynamics and Excitation-Inhibition Balance. J Neurophysiol 90:415–430.

Buzsáki G, Wang X-J (2012) Mechanisms of Gamma Oscillations. Annu Rev Neurosci 35:203–225.

Canolty RT, Edwards E, Dalal SS, Soltani M, Nagarajan SS, Kirsch HE, Berger MS, Barbaro NM, Knight RT (2006) High Gamma Power Is Phase-Locked to Theta Oscillations in Human Neocortex. Science 313:1626–1628.

Carbonnell L, Falkenstein M (2006) Does the error negativity reflect the degree of response conflict? Brain Res 1095:124–130.

Carp J, Compton RJ (2009) Alpha power is influenced by performance errors. Psychophysiology 46:336–343.

Crone NE, Miglioretti DL, Gordon B, Lesser RP (1998) Functional mapping of human sensorimotor cortex with electrocorticographic spectral analysis. II. Event-related synchronization in the gamma band. Brain J Neurol 121 (Pt 12):2301–2315.

Crone NE, Sinai A, Korzeniewska A (2006) High-frequency gamma oscillations and human brain mapping with electrocorticography. In: Progress in Brain Research (Klimesch CN and W, ed), pp 275–295 Event-Related Dynamics of Brain Oscillations. Elsevier. Available at: http://www.sciencedirect.com/science/article/pii/S0079612306590193.

Darvas F, Scherer R, Ojemann JG, Rao RP, Miller KJ, Sorensen LB (2010) High gamma mapping using EEG. NeuroImage 49:930–938.

Dixon WJ, Mood AM (1946) The Statistical Sign Test. J Am Stat Assoc 41:557–566.

Eickhoff SB, Heim S, Zilles K, Amunts K (2006) Testing anatomically specified hypotheses in functional imaging using cytoarchitectonic maps. NeuroImage 32:570–582.

Eickhoff SB, Paus T, Caspers S, Grosbras M-H, Evans AC, Zilles K, Amunts K (2007) Assignment of functional activations to probabilistic cytoarchitectonic areas revisited. NeuroImage 36:511–521.

Eickhoff SB, Stephan KE, Mohlberg H, Grefkes C, Fink GR, Amunts K, Zilles K (2005) A new SPM toolbox for combining probabilistic cytoarchitectonic maps and functional imaging data. NeuroImage 25:1325–1335.

Engbert R, Kliegl R (2003) Microsaccades uncover the orientation of covert attention. Vision Res 43:1035–1045.

Eriksen CW, Eriksen BA (1979) Target redundancy in visual search: Do repetitions of the target within thedisplay impair processing? Percept Psychophys 26:195–205.

Falkenstein M, Hohnsbein J, Hoormann J, Blanke L (1991) Effects of crossmodal divided attention on late ERP components. II. Error processing in choice reaction tasks. Electroencephalogr Clin Neurophysiol 78:447–455.

Ferrez PW, Millan J del R (2008) Error-Related EEG Potentials Generated During Simulated Brain #x2013;Computer Interaction. IEEE Trans Biomed Eng 55:923–929.

Fonov V, Evans A, McKinstry R, Almli C, Collins D (2009) Unbiased nonlinear average age-appropriate brain templates from birth to adulthood. NeuroImage 47, Supplement 1:S102.

Freeman WJ, Rogers LJ, Holmes MD, Silbergeld DL (2000) Spatial spectral analysis of human electrocorticograms including the alpha and gamma bands. J Neurosci Methods 95:111–121.

Fries P (2005) A mechanism for cognitive dynamics: neuronal communication through neuronal coherence. Trends Cogn Sci 9:474–480.

Gehring WJ, Goss B, Coles MGH, Meyer DE, Donchin E (1993) A Neural System for Error Detection and Compensation. Psychol Sci 4:385–390.

Gehring WJ, Knight RT (2000) Prefrontal–cingulate interactions in action monitoring. Nat Neurosci 3:516–520.

Goncharova II, McFarland DJ, Vaughan TM, Wolpaw JR (2003) EMG contamination of EEG: spectral and topographical characteristics. Clin Neurophysiol 114:1580–1593.

Hajcak G, McDonald N, Simons RF (2003) Anxiety and error-related brain activity. Biol Psychol 64:77–90.

Herrmann CS, Munk MHJ, Engel AK (2004a) Cognitive functions of gamma-band activity: memory match and utilization. Trends Cogn Sci 8:347–355.

Herrmann MJ, Römmler J, Ehlis A-C, Heidrich A, Fallgatter AJ (2004b) Source localization (LORETA) of the error-related-negativity (ERN/Ne) and positivity (Pe). Cogn Brain Res 20:294–299.

Holroyd CB, Coles MGH (2002) The neural basis of human error processing: reinforcement learning, dopamine, and the error-related negativity. Psychol Rev 109:679–709.

Howard MW, Rizzuto DS, Caplan JB, Madsen JR, Lisman J, Aschenbrenner-Scheibe R, Schulze-Bonhage A, Kahana MJ (2003) Gamma Oscillations Correlate with Working Memory Load in Humans. Cereb Cortex 13:1369–1374.

Jensen O, Kaiser J, Lachaux J-P (2007) Human gamma-frequency oscillations associated with attention and memory. Trends Neurosci 30:317–324.

Jerbi K, Freyermuth S, Dalal S, Kahane P, Bertrand O, Berthoz A, Lachaux J-P (2009) Saccade Related Gamma-Band Activity in Intracerebral EEG: Dissociating Neural from Ocular Muscle Activity. Brain Topogr 22:18–23.

Koelewijn T, van Schie HT, Bekkering H, Oostenveld R, Jensen O (2008) Motor-cortical beta oscillations are modulated by correctness of observed action. NeuroImage 40:767–775.

Kolev V, Falkenstein M, Yordanova J (2005) Aging and error processing - Time-frequency analysis of error-related potentials. J Psychophysiol 19:289–297.

Kopp B, Rist F, Mattler U (1996) N200 in the flanker task as a neurobehavioral tool for investigating executive control. Psychophysiology 33:282–294.

Kreilinger A, Neuper C, Müller-Putz GR (2012) Error potential detection during continuous movement of an artificial arm controlled by brain–computer interface. Med Biol Eng Comput 50:223–230.

Kucewicz MT, Berry BM, Kremen V, Brinkmann BH, Sperling MR, Jobst BC, Gross RE, Lega B, Sheth SA, Stein JM, Das SR, Gorniak R, Stead SM, Rizzuto DS, Kahana MJ, Worrell GA

(2017) Dissecting gamma frequency activity during human memory processing. Brain 140:1337–1350.

Luu P, Tucker DM, Makeig S (2004) Frontal midline theta and the error-related negativity: neurophysiological mechanisms of action regulation. Clin Neurophysiol 115:1821–1835.

Maier ME, di Pellegrino G, Steinhauser M (2012) Enhanced error-related negativity on flanker errors: Error expectancy or error significance? Psychophysiology 49:899–908.

Mann HB, Whitney DR (1947) On a Test of Whether one of Two Random Variables is Stochastically Larger than the Other. Ann Math Stat 18:50–60.

Mazziotta J et al. (2001) A probabilistic atlas and reference system for the human brain: International Consortium for Brain Mapping (ICBM). Philos Trans R Soc Lond B Biol Sci 356:1293–1322.

Milekovic T, Ball T, Schulze-Bonhage A, Aertsen A, Mehring C (2013) Detection of Error Related Neuronal Responses Recorded by Electrocorticography in Humans during Continuous Movements. PLoS ONE 8:e55235.

Moore DS, McCabe GP (1989) Introduction to the practice of statistics. New York, NY, US: W H Freeman/Times Books/ Henry Holt & Co.

Nieuwenhuis S, Ridderinkhof KR, Blom J, Band GPH, Kok A (2001) Error-related brain potentials are differentially related to awareness of response errors: Evidence from an antisaccade task. Psychophysiology 38:752–760.

Nieuwenhuis S, Ridderinkhof KR, Talsma D, Coles MGH, Holroyd CB, Kok A, Molen MW van der (2002) A computational account of altered error processing in older age: Dopamine and the error-related negativity. Cogn Affect Behav Neurosci 2:19–36.

Nottage JF, Morrison PD, Williams SCR, Ffytche DH (2013) A Novel Method for Reducing the Effect of Tonic Muscle Activity on the Gamma Band of the Scalp EEG. Brain Topogr 26:50–61.

Oldfield RC (1971) The assessment and analysis of handedness: The Edinburgh inventory. Neuropsychologia 9:97–113.

Pistohl T, Schulze-Bonhage A, Aertsen A, Mehring C, Ball T (2012) Decoding natural grasp types from human ECoG. NeuroImage 59:248–260.

Ridderinkhof KR, Vlugt Y de, Bramlage A, Spaan M, Elton M, Snel J, Band GPH (2002) Alcohol Consumption Impairs Detection of Performance Errors in Mediofrontal Cortex. Science 298:2209–2211.

Shibata T, Shimoyama I, Ito T, Abla D, Iwasa H, Koseki K, Yamanouchi N, Sato T, Nakajima Y (1999) Event-related dynamics of the gamma-band oscillation in the human brain: information processing during a GO/NOGO hand movement task. Neurosci Res 33:215–222.

Shiels K, Hawk LW (2010) Self-regulation in ADHD: The role of error processing. Clin Psychol Rev 30:951–961.

Smith MM, Weaver KE, Grabowski TJ, Rao RPN, Darvas F (2014) Non-invasive detection of high gamma band activity during motor imagery. Front Hum Neurosci 8 Available at: http://journal.frontiersin.org/article/10.3389/fnhum.2014.00817/abstract.

Spüler M, Bensch M, Kleih S, Rosenstiel W, Bogdan M, Kübler A (2012) Online use of error-related potentials in healthy users and people with severe motor impairment increases performance of a P300-BCI. Clin Neurophysiol 123:1328–1337.

Steinhauser M, Yeung N (2010) Decision Processes in Human Performance Monitoring. J Neurosci 30:15643–15653.

Tadel F, Baillet S, Mosher JC, Pantazis D, Leahy RM (2011) Brainstorm: A User-Friendly Application for MEG/EEG Analysis. Comput Intell Neurosci 2011:e879716.

Taylor SF, Stern ER, Gehring WJ (2007) Neural Systems for Error Monitoring: Recent Findings and Theoretical Perspectives. The Neuroscientist 13:160–172.

Thomson DJ (1982) Spectrum estimation and harmonic analysis. Proc IEEE 70:1055–1096.

Trujillo LT, Allen JJB (2007) Theta EEG dynamics of the error-related negativity. Clin Neurophysiol 118:645–668.

Whitham EM, Pope KJ, Fitzgibbon SP, Lewis T, Clark CR, Loveless S, Broberg M, Wallace A, DeLosAngeles D, Lillie P, Hardy A, Fronsko R, Pulbrook A, Willoughby JO (2007) Scalp electrical recording during paralysis: Quantitative evidence that EEG frequencies above 20 Hz are contaminated by EMG. Clin Neurophysiol 118:1877–1888.

Yordanova J, Falkenstein M, Hohnsbein J, Kolev V (2004) Parallel systems of error processing in the brain. NeuroImage 22:590–602.

Yuval-Greenberg S, Tomer O, Keren AS, Nelken I, Deouell LY (2008) Transient Induced Gamma-Band Response in EEG as a Manifestation of Miniature Saccades. Neuron 58:429–441.

Zavala B, Brittain J-S, Jenkinson N, Ashkan K, Foltynie T, Limousin P, Zrinzo L, Green AL, Aziz T, Zaghloul K, Brown P (2013) Subthalamic Nucleus Local Field Potential Activity during the Eriksen Flanker Task Reveals a Novel Role for Theta Phase during Conflict Monitoring. J Neurosci 33:14758–14766.

Tables

Table 1: Excerpt of studies about error-related spectral power modulations in EEG & MEG.

As frequency band definitions were not consistent amongst the publications, the respective definition is stated within parentheses.

Author / year	Signals	Error-related spectral modulations	Paradigm
Yordanova et al., 2004	64 EEG channels	**Delta (1.5-3.5 Hz)** amplitude increase during ERN/Ne component, **theta (4-8 Hz)** amplitude increase associated with erroneous motor execution.	Four-choice reaction task. 14 subjects (thereof 4 subjects rejected due to too low error rate).
Luu et al., 2004	128 EEG channels	**Theta power (4-7 Hz) increase** at midfrontal channels, starting with response, ending 400ms after ERN/Ne peak.	Forced-choice speeded response paradigm, 11 subjects.
Kolev et al., 2005	64 EEG channels	Error-specific **delta band (1.5-3.5 Hz)** power increase and phase locking. **Theta power (4-7 Hz)** increase after errors in young subjects, not in older subjects.	Four-choice reaction task. 10 “young” subjects (mean age 22.5±1.5 years), 11 “older” subjects (mean age 58.3±2.1 years).
Trujillo and Allen, 2007	25 EEG channels	**Theta power (4-7 Hz) increase** at midfrontocentral sites, 150ms prior to button press until 400ms after it. Stronger increase in non-phase-locked power than in phase-locked power.	Eriksen flanker task, 21 subjects. Stimuli: ‘SSSSS’, ‘HHHHH’, ‘SSHSS’, and ‘HHSHH’
Koelewijn et al., 2008	151 MEG sensors	**Beta power (15-35 Hz) depression** during erroneous task execution, then beta rebound	Motor error observation task. Effect sources identified as dorsal motor areas. 12 subjects (9m, 3f).
Carp and Compton, 2009	8 EEG channels	**Alpha power (10-14 Hz)** increase, then decrease in correct trials; absent in erroneous trials.	Stroop task; 81 subjects (46f, 35m).